Identification of Optimal Reduced Order Homogenization Models for Failure of Heterogeneous Materials

Paul Sparks, Caglar Oskay*

Department of Civil and Environmental Engineering
Vanderbilt University
Nashville, TN, 37235

Abstract

This manuscript presents a new methodology for the identification of optimal reduced order models for the inelastic and failure response of heterogeneous materials. The proposed methodology employs the eigendeformation-based reduced order homogenization approach. The identification of the optimal reduced order model is posed as an integer optimization problem and the genetic algorithm method is used to evaluate the optimization problem. A second optimization problem is posed to ensure that the errors associated with the optimal reduced order model are minimized through scaling of the failure parameters. The performance and capabilities of the optimal reduced order models identified based on the proposed approach are demonstrated by comparing model predictions with the computational homogenization method with full resolution of the material microstructure. Numerical simulations conducted using unidirectional reinforced matrix microstructures reveal that the reduced order models accurately describe the response characteristics of the composite material for a wide range of loading regimes.

Keywords: Reduced order modeling, Multiscale modeling, Heterogeneous materials, Optimization, Genetic algorithm.

1 Introduction

Computational homogenization is emerging as a powerful modeling and simulation tool for structures made of composite and heterogeneous materials. The computational homogenization method is based on the mathematical homogenization theory pioneered by Babuska [1], Bensoussan [2], Suquet [3], and Sanchez-Palencia [4]. The key characteristic of this method is that the macroscopic constitutive behavior of the heterogeneous material is provided by the numerical solution of a boundary value problem defined over the representative volume of the microstructure. The computational homogenization method has been successfully applied to evaluate the mechanical and functional behavior of materials with complex microstructures that include inelastic, viscous and damage effects [5, 6], geometric nonlinearities [7, 8] and multiphysics response [9, 10]. Recently, significant research is ongoing to extend the computational homogenization approach to model failure and cracking phenomena in composite materials [11–13].

*Corresponding Author: VU Station B#351831, 2301 Vanderbilt Place, Nashville, TN 37235. Email: caglar.oskay@vanderbilt.edu

One of the main challenges of computational homogenization is the computational complexity involved in solving boundary value problems at two (or more) scales. The issue of computational complexity is addressed using parallel implementation strategies, reduced order modeling at the coarse scale using high order (i.e., plate and shell) theories or reduced order modeling at the fine scales to efficiently evaluate the microscale response, as well as a combination of these three approaches. Parallelization of the computational homogenization [12, 14, 15] is natural and domain decomposition is readily applicable due to the local character of the microscale boundary value problems that are typically evaluated at the integration points of the macroscale grid. Model reduction at the coarse scale is achieved by exploiting the characteristics of the macroscopic domain. For instance, plate and shell theories have been recently employed to evaluate the response of thin structures with heterogeneous microstructure [16–19].

The third approach to reducing the computational cost of the computational homogenization method is to approximate the microscale boundary value problem with a reduced order representation. This approach finds its roots in the effective medium theory [20], which provides analytical or semi-analytical approximation to the microscale problem. More recently, computational reduced order models have been proposed to address complex microstructural topologies and nonlinear behavior. Major progress in reduced order modeling has been made using the boundary element method [21], the Voronoi cell method [22], the method of cells [23], the fast Fourier transforms [24], the network approximation method [25], the proper orthogonal decomposition [26] and the proper generalized decomposition [27]. Eigendeformation-based reduced order homogenization method has been shown to be another effective approach that can be applied to problems involving material nonlinearities [28–30], as well as interface decohesion at the microstructural scale [31, 32]. This approach employs the transformation field analysis [33, 34] and evaluates the nonlinear microscale problem using only a small set of unknowns through construction of microstructural influence functions and localization operators that are pre-computed using linear elastic microscale problems. Many reduced order approaches rely on representing the nonlinear response using a small number of functions spanning a basis with dimensions much smaller than the full scale microscale boundary value problem. Choosing the appropriate basis, as well as the order that can represent the fine scale response is therefore the critical question. The basis functions are typically reduced from the response of fully resolved microstructure problems subjected to a small number of load scenarios that the overall structure is expected to undergo. In nonlinear problems, the microstructure loading may significantly change through the course of the loading due to load redistribution. While the reduced order models are accurate in the load conditions at which they are derived, their performance at full load spectrum is not always accurate.

In this manuscript, we provide a methodology to identify optimal reduced order homogenization models for efficiently approximating the inelastic and failure response of heterogeneous materials. The reduced order modeling approach taken in this study is the eigendeformation-based reduced order homogenization method [31]. The identification of the optimal reduced order model lends itself as an integer optimization problem, which is evaluated using the genetic algorithm optimization technique. In particular, this manuscript addresses (1) how to identify the best reduced order basis for a given model order; (2) the effect of increasing the model order on the overall accuracy of the microscale computations; and, (3) the accuracy characteristics of the optimal reduced order models across a full load spectra beyond the loading directions at which the reduced order models are developed.

The remainder of the manuscript is organized as follows: The macroscale and microscale

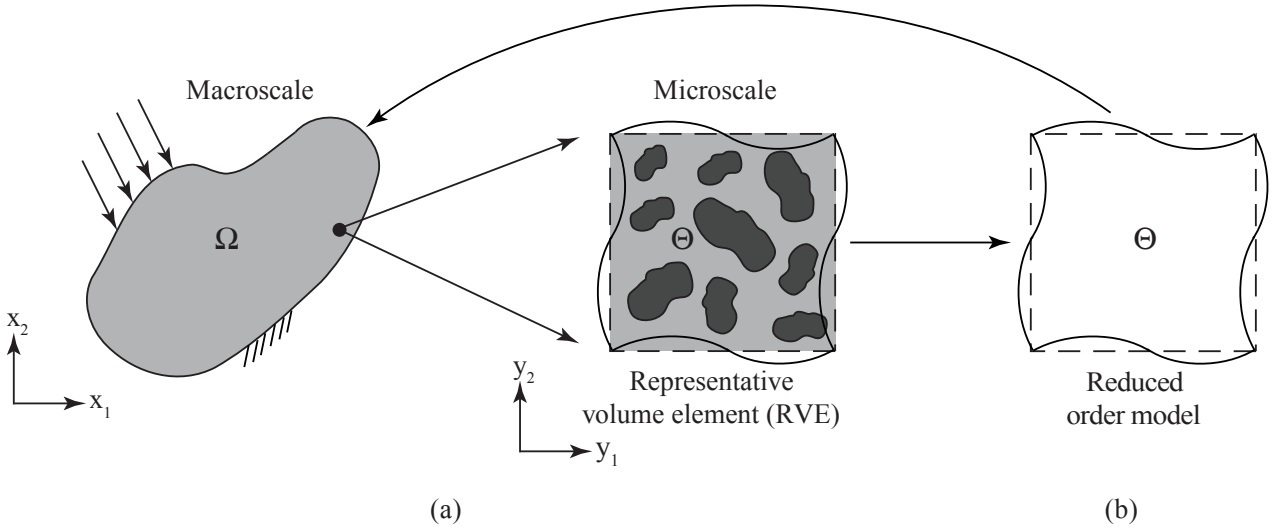

Figure 1: Macro- and microscopic structures.

problems in the context of the computational homogenization method is described in Section 2. Section 3 provides the reduced order model based on the eigendeformation-based reduced order homogenization method. In Section 4, the problem statement for the identification of the optimal reduced order model is provided. The solution methodology based on genetic algorithm and the details of the implementation of the identification problem is described. The numerical examples are discussed in Section 5. Section 6 provides the conclusions and future research in this area.

2 Computational Homogenization

We seek to model the inelastic deformation of a macroscopic domain, Ω, with a heterogeneous microstructure as illustrated in Fig. 1. The domain of the representative microstructure, Θ, consists of $c \geq 2$ constituent phases. The macroscopic domain is formed by the repetition of the microstructure. The macroscopic and microscopic domains are parameterized by the position vectors, $\mathbf{x}$ and $\mathbf{y}$, respectively. The response fields (e.g., displacement, strain, stress) are taken to be periodic with respect to Θ. The macro- and microscale position vectors are related by the small positive scaling parameter ζ (i.e., $0 < \zeta \ll 1$), such that $\mathbf{y} = \mathbf{x}/\zeta$.

The mathematical homogenization theory with multiple scales [2] is employed to formulate coupled boundary value problems that describe the response of an equivalent homogeneous domain (i.e., the macroscale problem) and the representative volume element (i.e., the microscale problem). To this extent, the displacement field is decomposed using a two-scale asymptotic expansion:

$$u_i\left(\mathbf{x},\mathbf{y},t\right) = \bar{u}_i\left(\mathbf{x},t\right) + \zeta u_i^1\left(\mathbf{x},\mathbf{y},t\right) \tag{1}$$

in which, $\bar{u}_i$ and u_i^1 are the macroscopic and microscopic displacement fields, respectively. The two-scale decomposition of the displacement field is substituted in the governing equations of equilibrium and asymptotic analysis is employed to decompose the governing equations into the macro- and microscale counterparts [31].

2.1 Macroscale problem

Applying the two-scale asymptotic decomposition into the equilibrium equations, considering the $O(1)$ terms and averaging over the representative volume element (RVE) leads to the following macroscale equilibrium equation defined over the macroscopic domain, Ω:

$$\bar{\sigma}_{ij,x_j}(\mathbf{x},t) + \bar{b}_i(\mathbf{x},t) = 0 \tag{2}$$

in which, $\bar{\sigma}_{ij}$ and $\bar{b}_i$ denote the macroscopic stress tensor and body force, respectively, which are volume-averaged over the domain of the RVE, Θ:

$$\bar{\sigma}_{ij}(\mathbf{x},t) = \langle \sigma_{ij} \rangle \tag{3}$$
$$\bar{b}_i(\mathbf{x},t) = \langle b_i \rangle \tag{4}$$

where, the Macaulay brackets are defined as:

$$\langle \cdot \rangle = \frac{1}{|\Theta|} \int_{\Theta} (\cdot) d\mathbf{y} \tag{5}$$

$|\Theta|$ is the volume of the RVE.

The stress field is expressed as:

$$\sigma_{ij}(\mathbf{x},\mathbf{y},t) = L_{ijkl}(\mathbf{y}) \left[\bar{\epsilon}_{kl}(\mathbf{x},t) + u^1_{(k,y_l)}(\mathbf{x},\mathbf{y},t) - \mu_{kl}(\mathbf{x},\mathbf{y},t) \right] \tag{6}$$

where, L_{ijkl} is the fourth order tensor of elastic moduli that vary within the RVE due to material heterogeneity. L_{ijkl} is taken to be symmetric and strongly elliptic. $\bar{\epsilon}_{ij} = \bar{u}_{(i,x_j)}$ is the macroscopic strain tensor; a subscript comma denotes differentiation, parentheses in the subscript denotes a symmetric differentiation. Small strain kinematics with additive split of the strain tensor is assumed: $\epsilon_{ij} = \epsilon^e_{ij} - \mu_{ij}$, where ϵ^e_{ij} is the elastic strain and μ_{ij} is the history-dependent inelastic strain tensor present due to one or a combination of plastic, viscous, damage and thermal processes, described in terms of internal state variables. In this manuscript, the inelastic processes are modeled using a scalar continuum damage mechanics model for simplicity. The evolution equations for the damage model are explained below. The boundary conditions of the macroscale problem are defined as:

$$\bar{u}_i(\mathbf{x},t) = g_i(\mathbf{x},t)\,; \quad \mathbf{x} \in \Gamma_u \tag{7}$$
$$\bar{\sigma}_{ij}(\mathbf{x},t)\, n_j = t_i(\mathbf{x},t)\,; \quad \mathbf{x} \in \Gamma_t \tag{8}$$

in which, g_i is the boundary displacement data prescribed on $\Gamma_u \subset \partial\Omega$; and, t_i is the boundary traction data prescribed on $\Gamma_t \subset \partial\Omega$, such that $\Gamma_u \cap \Gamma_t = \emptyset$ and $\Gamma_u \cup \Gamma_t = \partial\Omega$. The prescribed boundary conditions are taken to vary with respect to the macroscopic scale only and are constant with respect to the microscopic coordinates.

2.2 Microscale problem

Applying the two-scale asymptotic decomposition into the equilibrium equations, considering the $O(\zeta^{-1})$ terms leads to the following microscale equilibrium equation defined over the RVE domain, Θ:

$$\sigma_{ij,y_j}(\mathbf{x},\mathbf{y},t) = 0 \tag{9}$$

where, σ_{ij} is given in Eq. 6. Equation 9 is evaluated for the microscale displacement field, u_i^1, where the macroscopic strain, $\bar{\epsilon}_{ij}$ acts as the loading function for the microscale problem. The boundary condition of the microscale problem is taken to be periodic. For a rectangular cuboidal shaped RVE domain, the boundary is split into n_{sd} subdomains denoted by Γ_ξ, where $n_{\text{sd}} = 2$ or 3 is the number of spatial dimensions. Each boundary subdomain is a pair of parallel faces of the RVE boundary. The periodic boundary conditions are expressed as:

$$u_i^1(\mathbf{y}, t) = u_i^1(\mathbf{y} - l_\zeta \mathbf{n}_\xi, t); \quad \mathbf{y} \in \Gamma_\xi; \quad \xi = 1, \ldots, n_{\text{sd}} \tag{10}$$

in which, $\mathbf{n}_\xi$ is the unit outward normal on Γ_ξ, and l_ξ is the length of the RVE along $\mathbf{n}_\xi$. Zero microscale displacement is imposed at the vertices of the RVE domain to restrict rigid body motion.

3 Reduced Order Homogenization

When solving linear problems, the linearity of the microscale displacement field with respect to the macroscopic strains is exploited to pose the microscale problem in terms of a third order influence function, H_{ikl} (i.e., $u_i^1(\mathbf{x}, \mathbf{y}) = H_{ikl}(\mathbf{y})\,\bar{\epsilon}_{kl}(\mathbf{x})$). The macroscale stress is then a function of H_{ikl}. The influence function is computed numerically and then employed in the evaluation of the macroscale problem. In nonlinear problems, the microscale displacement field is a nonlinear and typically history-dependent function of the macroscale strain field. Therefore, a separate microscale problem is assigned to each integration point of a macroscale problem and evaluated for every load increment and iteration of a macroscale analysis. The computational burden in this approach is tremendous in case of large structural simulations or when the microstructure is complex. We employ the eigendeformation-based reduced order homogenization approach [31, 32] to develop a reduced order model for efficiently solving for the microscale response. The microscopic displacement field is expressed as:

$$u_i^1(\mathbf{x}, \mathbf{y}, t) = H_{ikl}(\mathbf{y})\,\bar{\epsilon}_{kl}(\mathbf{x}, t) + \int_\Theta h_{ikl}(\mathbf{y}, \hat{\mathbf{y}})\,\mu_{kl}(\mathbf{x}, \hat{\mathbf{y}}, t)\,d\hat{\mathbf{y}} \tag{11}$$

The inelastic influence function, h_{ikl}, consists of the particular solutions of the RVE and is approximated by numerical solutions of the linear elastic RVE problems [31].

The inelastic strain field is expressed as:

$$\mu_{ij}(\mathbf{x}, \mathbf{y}, t) = \sum_{\alpha=1}^{n} N^{(\alpha)}(\mathbf{y})\,\mu_{ij}^{(\alpha)}(\mathbf{x}, t) \tag{12}$$

where, $N^{(\alpha)}$ are the mesomechanical shape functions; n is the order of discretization (also referred to as the model order in this manuscript), and $\mu_{ij}^{(\alpha)}$ are the microscopically nonlocal inelastic strain coefficients:

$$\mu_{ij}^{(\alpha)}(\mathbf{x}, t) = \int_\Theta \varphi^{(\alpha)}(\mathbf{y})\,\mu_{ij}(\mathbf{x}, \mathbf{y}, t)\,d\mathbf{y} \tag{13}$$

in which, $\varphi^{(\alpha)}$ are mesomechanical weight functions. Employing Eqs. 11, 12, and 1, a kinematic relationship between the nonlocal inelastic strain coefficients and nonlocal total strain coefficient is obtained:

$$\epsilon_{ij}^{(\alpha)}(\mathbf{x}, t) = A_{ijkl}^{(\alpha)}\bar{\epsilon}(\mathbf{x}, t) + \sum_{\beta=1}^{n} P_{ijkl}^{(\alpha\beta)}\mu_{kl}^{(\beta)}(\mathbf{x}, t) \tag{14}$$

where, $\epsilon_{ij}^{(\alpha)}$ is defined analogous to Eq. 13, and:

$$A_{ijkl}^{(\alpha)} = I_{ijkl} + \int_{\Theta} \varphi^{(\alpha)}(\mathbf{y})\, G_{ijkl}(\mathbf{y})\, d\mathbf{y} \tag{15}$$

$$P_{ijkl}^{(\alpha\beta)} = \int_{\Theta}\int_{\Theta} \varphi^{(\alpha)}(\mathbf{y})\, g_{ijkl}(\mathbf{y},\hat{\mathbf{y}})\, N^{(\beta)}(\hat{\mathbf{y}})\, d\hat{\mathbf{y}} d\mathbf{y} \tag{16}$$

in which, $G_{ijkl} = H_{(ikl,y_j)}$ and $g_{ijkl} = h_{(ikl,y_j)}$ are elastic and inelastic polarization tensors, respectively; and, I_{ijkl} the fourth order identity tensor. The evolution of the inelastic strains is modeled in terms of the nonlocal variables. In the functional form:

$$\dot{\mu}_{ij}^{(\alpha)} = f\left(\mu_{ij}^{(\alpha)}, \epsilon_{ij}^{(\alpha)}, \sigma_{ij}^{(\alpha)}, \mathbf{h}^{(\alpha)}\right) \tag{17}$$

where, $\sigma_{ij}^{(\alpha)}$ is the nonlocal stress coefficients defined analogous to Eq. 13 and using Eq. 6, and $\mathbf{h}^{(\alpha)}$ denotes additional internal state variables defining the evolution of the inelastic process. Equation 17 along with Eq. 14 are evaluated to obtain $\mu_{ij}^{(\alpha)}$ for a prescribed macroscopic strain state. The computed inelastic strain field satisfies the microscale equilibrium *a-priori* via the influence functions. The evaluation of $\mu_{ij}^{(\alpha)}$ therefore provides an approximation to the solution of the microscale problem. The specific form of the evolution equations (Eq. 17) requires that the nonlocal inelastic strain coefficients describe the inelastic processes at a subdomain occupied by a single constituent phase. Let $\Theta_i \subset \Theta$ denote the domain of phase i ($1 \leq i \leq c$) within the RVE. Each phase is decomposed into n_i non-overlapping parts: $\Theta_i = \cup_{j=1}^{n_j} \Theta_i^{(j)}$, where $\Theta_i^{(j)} \cap \Theta_i^{(k)} = \emptyset$ if $j \neq k$. We further define a part of the RVE, $\Theta^{(\alpha)} = \Theta_i^{(j)}$ such that $\alpha = j + \sum_{k=1}^{i-1} n_k$. The mesomechanical shape and weight functions are taken to be piecewise constant within the RVE domain:

$$N^{(\alpha)}(\mathbf{y}) = \begin{cases} 1 \text{ if } \mathbf{y} \in \Theta^{(\alpha)} \\ 0 \text{ elsewhere} \end{cases} \tag{18}$$

$$\varphi^{(\alpha)}(\mathbf{y}) = \frac{1}{\left|\Theta^{(\alpha)}\right|} N^{(\alpha)}(\mathbf{y}) \tag{19}$$

where, $\left|\Theta^{(\alpha)}\right|$ is the volume of part $\Theta^{(\alpha)}$. This set of shape functions clearly forms an orthonormal basis and satisfies the partition of unity property of the reduced order basis.

3.1 Continuum damage mechanics model

In this study, the evolution of the inelastic strain is modeled using a scalar continuum damage mechanics model:

$$\mu_{ij}^{(\alpha)} = \omega^{(\alpha)} \epsilon_{ij}^{(\alpha)} \tag{20}$$

in which, $\omega^{(\alpha)} \in [0,1)$ is the damage variable with $\omega^{(\alpha)} = 0$ and $\omega^{(\alpha)} \to 1$ indicate the states of no damage and complete loss of load carrying capacity within part $\Theta^{(\alpha)}$, respectively. The evolution of the damage variable follows:

$$\omega^{(\alpha)}(\mathbf{x},t) = \Phi\left(\kappa^{(\alpha)}(\mathbf{x},t)\right); \quad \frac{\partial\Phi\left(\kappa^{(\alpha)}\right)}{\partial\kappa^{(\alpha)}} \geq 0 \tag{21}$$

where,

$$\kappa^{(\alpha)}(\mathbf{x},t) = \max\left\{ v^{(\alpha)}(\mathbf{x},\tau) \middle| \tau \leq t \right\} \tag{22}$$

$v^{(\alpha)}$ is the nonlocal damage equivalent strain defined based on the strain-based damage theory [35] as:

$$v^{(\alpha)}(\mathbf{x},t) = \sqrt{\frac{1}{2}\epsilon_{ij}^{(\alpha)} L_{ijkl}^{(\alpha)} \epsilon_{kl}^{(\alpha)}} \tag{23}$$

$L_{ijkl}^{(\alpha)}$ is the tensor of elastic moduli of the constituent phase occupying $\Theta^{(\alpha)}$. By strong ellipticity of $L_{ijkl}^{(\alpha)}$, the nonlocal damage equivalent strain is non-negative.

The evolution of phase damage as a function of the phase deformation function follows the arctangent law [28]

$$\Phi^{(\alpha)} = \frac{\operatorname{atan}\left(a^{(\alpha)}\kappa^{(\alpha)}(\mathbf{x},t) - b^{(\alpha)}\right) + \operatorname{atan}\left(b^{(\eta)}\right)}{\pi/2 + \operatorname{atan}\left(b^{(\alpha)}\right)} \tag{24}$$

in which, $a^{(\alpha)}$ and $b^{(\beta)}$ are material parameters.

Considering the particular form of the scalar damage model (Eq. 20), combining with Eq. 14 and using the shape and weight functions defined as in Eqs. 18 and 19, the nonlocal inelastic strain coefficients are expressed in the following algebraic form ($\forall \alpha = 1, 2, \ldots, n$):

$$\sum_{\beta=1}^{n} \left[\delta_{\alpha\beta} I_{ijkl} - P_{ijkl}^{(\alpha\beta)} \omega^{(\alpha)}(\mathbf{x},t)\right] \mu_{kl}^{(\beta)}(\mathbf{x},t) - \omega^{(\alpha)}(\mathbf{x},t) A_{ijkl}^{(\alpha)} \bar{\epsilon}_{kl}(\mathbf{x},t) = 0 \tag{25}$$

where, $\delta_{\alpha\beta}$ is Kronecker delta.

4 Identification of Optimal Reduced Order Model

In this section, we formulate the problem of identifying the optimal reduced order models and provide the solution strategy for the identification problem based on optimization with the genetic algorithm. A separate optimization problem is posed to scale the parameters of the optimal reduced order models and minimize the modeling errors.

4.1 Problem statement

Consider a finite element discretization of the RVE domain, $\Lambda = \{e_1, e_2, \ldots, e_{n_{\text{el}}}\}$, where e_i denotes a finite element; and, n_{el} the total number of finite elements. A reduced order model of order n is represented by an index set (i.e., individual) $X = \{X_1, X_2, \ldots, X_{n_{\text{el}}}\}$ such that $X_i = \alpha$ if $e_i \subset \Theta^{(\alpha)}$.

Let σ_{ref} and σ_X be the response metrics computed using the computational homogenization method (i.e., reference model) with full resolution of the microstructure and using the reduced order model, X of order n, respectively. The identification of the optimal reduced order model consists of minimizing the discrepancy between the response metrics computed by the reference and the reduced order models:

Find $X^* \in \chi^n \equiv \{X \mid 1 \leq X_i \leq n\}$, which satisfies:

$$\mathbb{F}(X^*) = \min_{X \in \chi^n} \|\sigma_{ref} - \sigma_X\|_{(\cdot)} \tag{26}$$

where χ^n is a set of all possible individuals that define a reduced order model with model order, n, and X^* is the optimal reduced order model. In this manuscript, the macroscopic

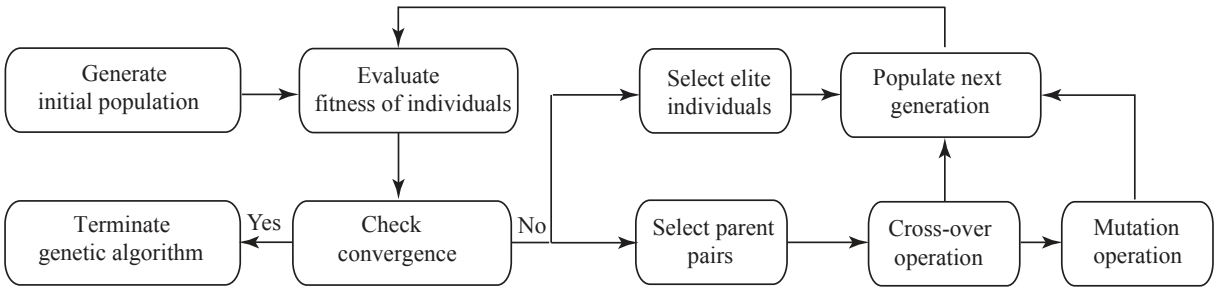

Figure 2: Structure of the identification strategy using genetic algorithm.

stress-strain response when subjected to n_{load} loading conditions are taken as the response metric. The objective function becomes:

$$\mathbb{F}(X^*) = \min_{X \in \chi^n} \sum_{\kappa=1}^{n_{load}} \left\| \bar{\sigma}_{ref}^{(\kappa)}(\bar{\epsilon}_{ij}) - \bar{\sigma}_{X}^{(\kappa)}(\bar{\epsilon}_{ij}) \right\|_2 \tag{27}$$

where $\| \cdot \|_2$ denotes L_2 norm, $\bar{\sigma}_{ref}^{(\kappa)}$ and $\bar{\sigma}_{X}^{(\kappa)}$ are the histories of the macroscopic Von-Mises stress under the load case, κ, computed using the reference model and the reduced order model, respectively.

Each individual in the space χ^n represents a reduced order model of order n but the representation is non-unique: multiple individuals may represent the same reduced order model. This difficulty is alleviated by ordering of the parts, $\Theta^{(\alpha)}$. An example is the ascending order of the parts such that the element with the smallest label in each part $\Theta^{(\alpha)}$ increases with α: Let $\Lambda^{(\alpha)} = \{e_i \,|\, e_i \in \Theta^{(\alpha)}; 1 \leq i \leq n_{\text{el}}\}$ be the set of the finite elements spanning the part $\Theta^{(\alpha)}$ ordered such that $\Lambda^{(\alpha)}(i) > \Lambda^{(\alpha)}(i-1)$; $2 \leq i \leq n_{\text{el}}$. We reorder the parts such that $\Lambda^{(1)}(1) < \Lambda^{(2)}(1) < \ldots < \Lambda^{(n)}(1)$.

The model order of n is ensured by assigning at least one element to each part. By this constraint a model of order m cannot be represented by a model of a higher order $n > m$.

4.2 Genetic algorithm

The optimal reduced order models are identified using the genetic algorithm optimization method. Identification of the optimal reduced order model is an integer optimization problem, since each individual in the search space, χ^n, is represented using an integer set. The gradient-based optimization methods [36], commonly employed in many engineering problems, are typically for real valued problems and therefore not applicable. Evolutionary (e.g., genetic) algorithms provide an effective approach to solving nonlinear integer optimization problems [37–39], since they are based on function evaluations only (no gradient information is needed or convexity required), they are global optimizers (local minima do not necessarily compromise the solution) and represent the search space digitally, naturally fitting integer representations. The literature in evolutionary algorithms is vast and they have been successfully employed in a variety of problems [39, 40]. Genetic algorithms typically consist of: (a) creation of a set of individuals (i.e., population) by random sampling of the search space; (b) assessment of the fitness of the individuals within the population based on objective function evaluation, where the fitness of an individual is inversely proportional to the corresponding objective function; and, (c) creation of a set of new individuals from the previous population (i.e., generation)

based on the fitness of the individuals. Assessment of the fitness and creation of subsequent generations are repeated until an individual with the desired fitness (i.e., the extremum of the objective function) is achieved up to the chosen tolerance.

The structure of the genetic algorithm employed in this manuscript is illustrated in Fig. 2. The algorithm is initiated by creating the initial population of individuals ($P = \{X^1, X^2, \ldots, X^{n_{pop}}\}$), where X^i denotes an individual; and, n_{pop} the total number of individuals in the population. The initial population is randomly generated. The fitness of each individual in the population is computed, where the fitness is defined as the inverse of the objective function provided in Eq. 27.

The creation of the next generation of the population consists of: (1) the selection of a number of parent pairs from the current population for the cross-over operation; (2) the mutation of some individuals in the population; and, (3) the selection of elite individuals for inclusion in the next generation. The roulette wheel algorithm is employed in the selection of the parent pairs. In the roulette wheel algorithm, each individual within the population is assigned a probability of selection that is proportional to its fitness value. The parent pairs are randomly chosen from the population based on the assigned probabilities [41]. The cross-over operation consists of the generation of two offsprings from each parent pair using the integer representation (chromosome) of each individual. The chromosome of each parent is split into two parts at a randomly selected locus and the chromosome fragments are interchanged between the two parents to generate two new chromosomes (the offsprings). A number of offsprings resulting from the cross-over operations are subjected to mutation, which consists of replacing a targeted gene from the chromosome of an offspring. The selection of the individual to be mutated, the gene that will be targeted and the new value of the gene are all randomly chosen. The mutation operation reduces the probability of convergence to a local minimum by including random individuals into the search space at each generation. A number of elite individuals with the highest fitness values within the populations are passed on to the next generation without change.

New generations are created until a convergence criterion is satisfied. Two convergence criteria are employed in this study. The first criterion indicates convergence when the fitness of the best individual in the current generation is less than a predefined tolerance. The second criterion indicates convergence when the change in the average fitness of the population remains under a specified tolerance for a predefined number of generations (i.e., stall generations).

The genetic algorithm optimization for the identification of the optimal reduced order model is implemented using Matlab's global optimization toolbox. The general structure of the implementation at a given genetic algorithm step is illustrated in Figure 3. The genetic algorithm is implemented using a parallel solution strategy for computational efficiency. The computational cost of the identification problem is primarily due to the fitness evaluations, which consist of solving the multiscale boundary value problems. The population at a generation is split into p equal subsets (batches). The fitness of the individuals in the batches are evaluated concurrently using p compute nodes. At each fitness evaluation of an individual within a batch, the coefficient tensors for the reduced order model represented by the individual is computed. The genetic algorithm code communicates with a commercial finite element software (Abaqus) to conduct numerical simulations using the reduced order model. The user supplied subroutine functionality of Abaqus (UMAT) is used to incorporate the reduced order model into the Abaqus framework. The reference simulations based on the computational homogenization method is conducted *a-priori*, and appropriate data is stored in a file for access during fitness computation.

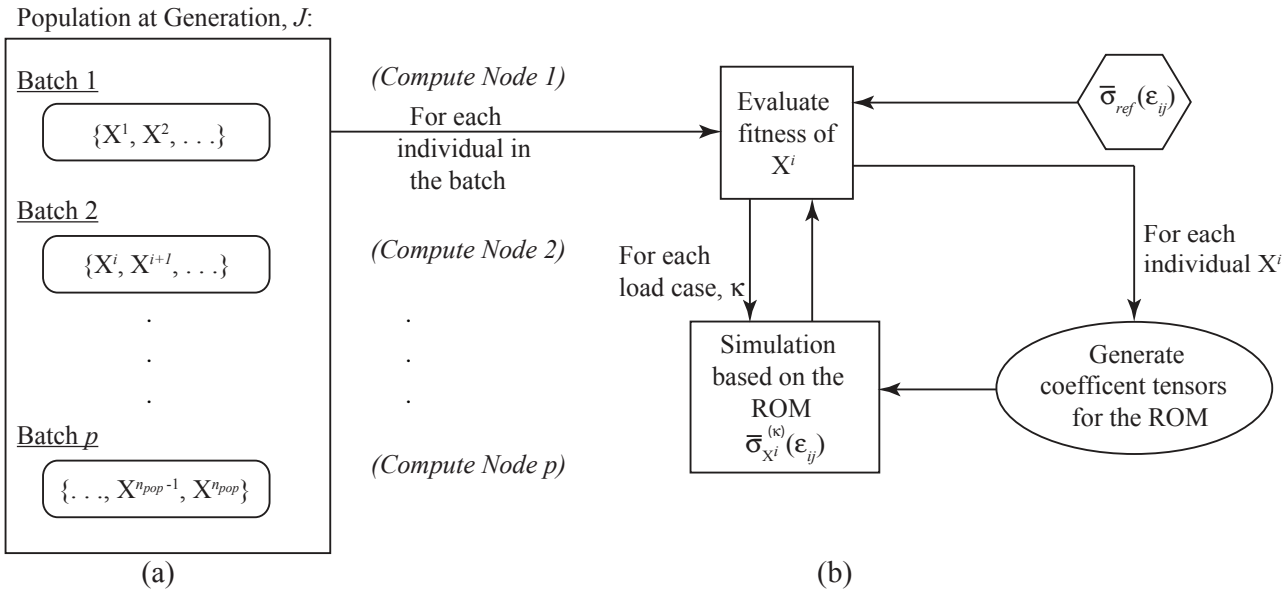

Figure 3: Implementation of the genetic algorithm: (a) parallel execution of the fitness evaluation; and, (b) strategy for evaluating the fitness of an individual.

4.3 Parameter scaling

The predictions of the reduced order models based on eigendeformation-based reduced order homogenization approach typically overestimate the strength properties. While the optimal reduced order model identification based on the methodology described above provides the best model among all possible models of the same order, the accuracy of the model can be improved by adjusting the model parameters. Let $\mathbf{s}$ be a vector of scaling constants associated with the material parameters of the microstructural constituents. The problem of identifying the parameter scaled optimal reduced order model is defined as:

Find the scaling constants, $\mathbf{s}^*$, which satisfies:

$$\mathcal{F}(\mathbf{s}^*) = \min_{s} \sum_{\kappa=1}^{n_{load}} \left\| \bar{\sigma}_{ref}^{(\kappa)}(\bar{\epsilon}_{ij}) - \bar{\sigma}_{X^*}^{(\kappa)}(\bar{\epsilon}_{ij}; \mathbf{s}) \right\|_2 \tag{28}$$

where $\bar{\sigma}_{X^*}^{(\kappa)}(\bar{\epsilon}_{ij}; \mathbf{s})$ is the constitutive response of the optimal reduced order model using the parameter set, $\mathbf{s}$. The identification problem constitutes nonlinear optimization with real valued parameters. Gradient based and evolutionary optimization methods are applicable in the evaluation of this problem.

The continuum damage mechanics model employed in this study includes two parameters for each microstructural constituent: $a^{(\alpha)}$ and $b^{(\alpha)}$. $a^{(\alpha)}$ controls the degree of brittleness at a material point at failure, whereas $b^{(\alpha)}$ controls the strength of the constituents. For a microstructure with two constituents (e.g., fiber and matrix), the parameter set is: $\mathbf{s} = \{s_a^{(m)}, s_b^{(m)}, s_a^{(f)}, s_b^{(f)}\}$. In the numerical examples considered in this study, the parameter scaling (Eq. 28) is evaluated for a single parameter $b^{(m)}$ by employing the Nelder-Mead simplex method.

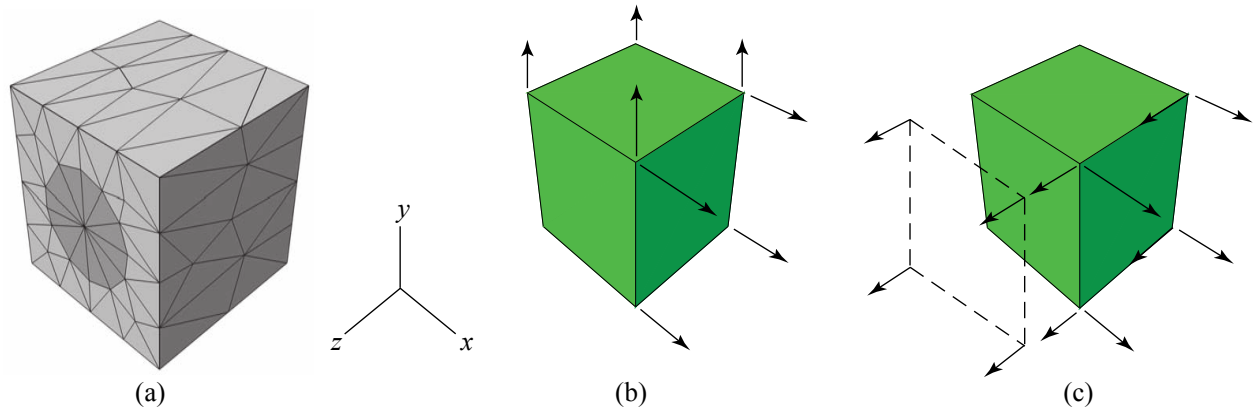

Figure 4: Geometry and discretization of the numerical example. (a) Microstructure; (b) Macrostructure subjected to biaxial tensile loading; (c) Macrostructure subjected to combined biaxial tensile and shear loading.

5 Numerical Examples

Numerical verification experiments were conducted to assess the capability of the proposed approach in identifying reduced order models under biaxial and triaxial loading conditions. The performance of the optimal reduced order models are compared to the direct numerical simulations based on the computational homogenization method, which constitutes the best solution that can be obtained by the reduced order models, since they are derived based on computational homogenization.

Numerical verification analyses are conducted by considering a unidirectional reinforced matrix microstructure with geometry, the discretization and the loading conditions are shown in Fig. 4. The finite element discretization of the unit cell consists of 351 tetrahedra. The matrix and the reinforcements are discretized using 251 and 98 elements, respectively. A unit cube discretized using a single hexahedral finite element constitutes the macroscale domain. The volume fraction of the reinforcement within the unit cell is 40%.

The numerical verifications consist of the identification of the optimal reduced order model partitioning based on a small number of load cases, which is then followed by parameter scaling and assessment of model performance using a wider range of loading conditions. A reduced order model is named based on the load cases employed in the identification step and the model order, n. T_i and S_{ij} denote uniaxial loading along the i-direction ($i = x, y, z$) and shear loading along the ij-direction, respectively. For instance, model T_x-S_{xz}-4 indicates a model of order 4 ($n = 4$) identified based on uniaxial tensile loading in the x-direction and shear loading in xz-direction (i.e., $n_{load} = 2$).

The parameters associated with the genetic algorithm are identical for all numerical experiments considered. The population size, n_{pop}, is taken to be 100. The predefined tolerance for convergence due to the fitness of the best individual is taken to be 100. The number of stall generations is set to 40 and the tolerance for convergence due to stall is set to 1e-6. The mutation ratio, which is the portion of the population that is mutated at each generation, is set to 0.01. The identification analyses are conducted using eight parallel compute nodes ($p = 8$).

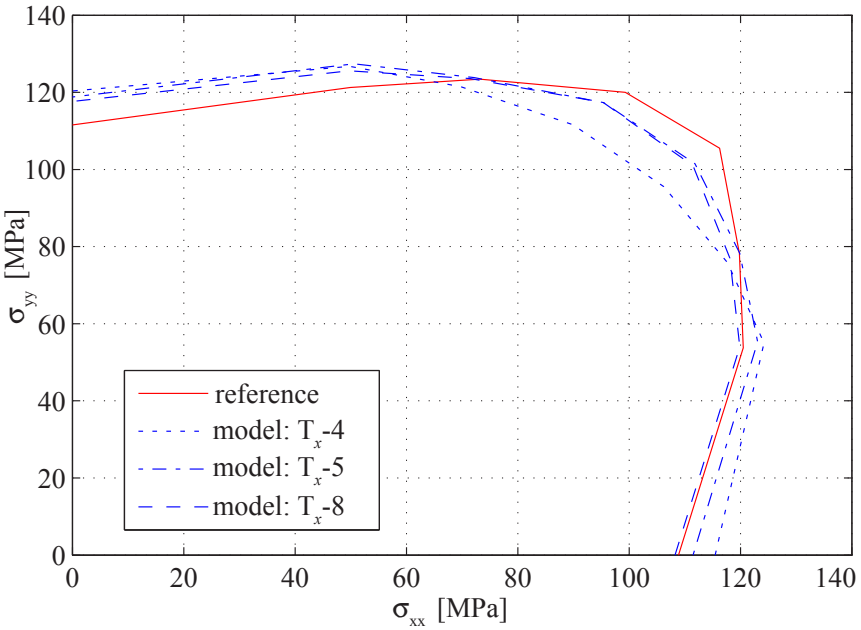

Figure 5: Failure envelopes for models T_x-4, T_x-5 and T_x-8 when subjected to tensile loading in x- and y-directions.

5.1 Biaxial tensile loading

The performance of the reduced order models are assessed under the condition of biaxial loading perpendicular to the direction of the reinforcement. The elastic modulus and Poisson's ratio for the reinforcements are $E^{(f)} = 200$ GPa and $\nu^{(f)} = 0.3$, and for the matrix are $E^{(m)} = 6$ GPa and $\nu^{(m)} = 0.3$. The reinforcement is taken to be linear elastic, whereas the matrix is modeled using the continuum damage mechanics model with the material parameters of $a^{(m)} = 32.0$ and $b^{(m)} = 16.3$. Each part within the matrix phase is taken to have the same material parameters. In all configurations considered, the entire reinforcement phase is taken to be a single part.

Figure 5 illustrates the accuracy of three reduced order models identified under uniaxial tensile loading in the x-direction. The stress envelopes computed using parameter-scaled models T_x-4, T_x-5 and T_x-8 display a reasonable match with the failure envelope computed using the reference computational homogenization method. The parameter scaling constants for models T_x-4, T_x-5 and T_x-8 are 0.87, 0.93 and 0.93, respectively. The modeling error after parameter scaling are respectively, 7.4%, 5.6% and 5.4% for the three models considered. A slight increase in the accuracy is observed with increasing model order for reduced order models with parameter scaling. The increase in accuracy as a function of model order is more pronounced in unscaled models with modeling errors of 17%, 11% and 9.7% for models T_x-4, T_x-5 and T_x-8, respectively, yet the impact of parameter scaling on the model accuracy is evident.

Figure 6 shows the failure envelopes of the three additional reduced order models identified under the combined uniaxial tension in the x- and y-directions (i.e., n_{load}=2) compared to the reference simulations after (Fig. 6a) and before (Fig. 6b) parameter scaling. The model errors prior to parameter scaling are 11.2%, 8.2% and 9.1% for T_x-T_y-4, T_x-T_y-5 and T_x-T_y-8, respectively, whereas the model errors with parameter scaling are respectively, 6.1%, 4.8% and 5.5%. The failure envelopes computed by the unscaled reduced order models clearly show

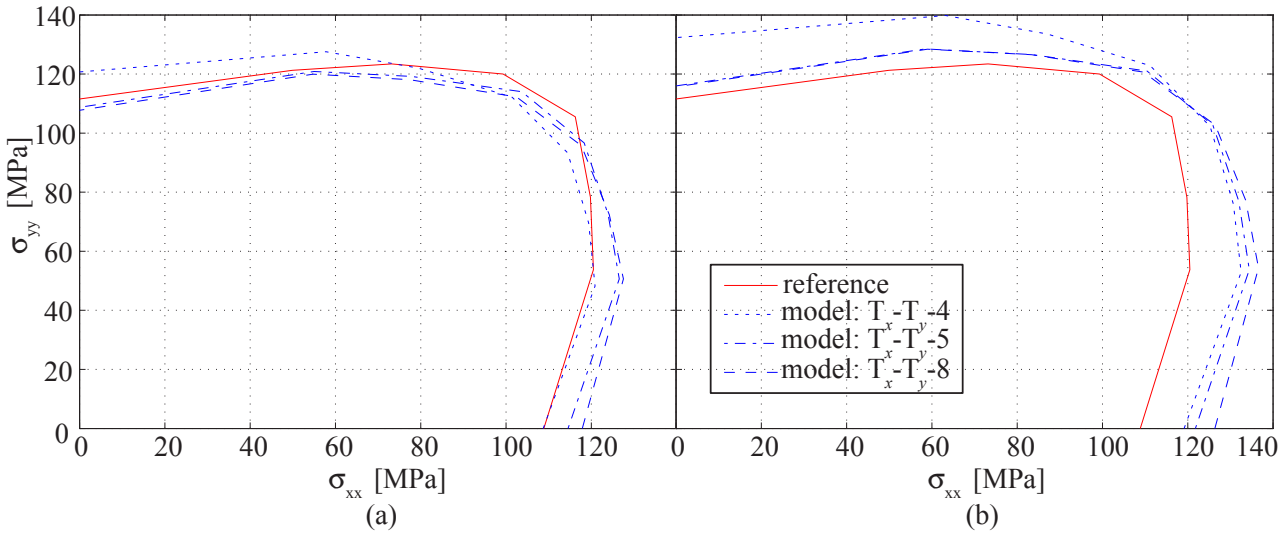

Figure 6: Failure envelopes for models T_x-T_y-4, T_x-T_y-5 and T_x-T_y-8 when subjected to tensile loading in x- and y-directions: (a) after parameter scaling; (b) before parameter scaling.

stiff response compared to the computational homogenization model, despite similar shape of the envelope and parameter scaling provides a significant improvement on the accuracy of the models. The errors clearly indicate that the accuracy is a non-monotonic function of the model order, and T_x-T_y-5 marginally outperforms T_x-T_y-8. Higher model orders do not include lower orders as subsets as each part is constrained to contain at least a single finite element. The optimal reduced order model partitions at orders 4, 5, and 8 are shown in Fig. 7. The model performance of the reduced order models identified using a single load case is comparable to that with two load cases due to the symmetry of the unit cell with respect to the loading directions. The ideal failure envelope is circular because of the symmetry of the microstructure with respect to the loading considered. The failure envelopes computed using the reference model as well as the reduced order models deviate from the circular shapes due to the relatively coarse discretization of the microstructure.

Figure 8 illustrates the stress-strain response as computed using the models T_x-T_y-4, T_x-T_y-5 and T_x-T_y-8, and the computational homogenization model when subjected to uniaxial loading (Fig. 8a-b) and under the biaxial loading with prescribed displacement ratio of $g_x/g_y = 1.5$ (Fig. 8c-d). In addition to accurately capturing the ultimate strength, the reduced order models capture the entire stress-strain response.

5.2 Combined biaxial tensile and shear loading

In the current example, we develop a reduced order model for laminated unidirectional reinforced composites. In laminated composites, the plies are typically subjected to a combined state of normal stresses along the reinforcement and transverse directions as well as shear stresses that develop due to the mismatch between neighboring ply orientations. A graphite fiber (IM-7) reinforced epoxy (977) resin is considered. The elastic modulus and Poisson's ratio for the reinforcements are $E^{(f)} = 263$ GPa and $\nu^{(f)} = 0.32$, and for the matrix are $E^{(m)} = 3.55$ GPa and $\nu^{(m)} = 0.35$. Damage is considered in both matrix and fiber phases with the material parameters of $a^{(m)} = 0.1$ and $b^{(m)} = 65$ for the matrix phase and $a^{(f)} = 0.1$ and

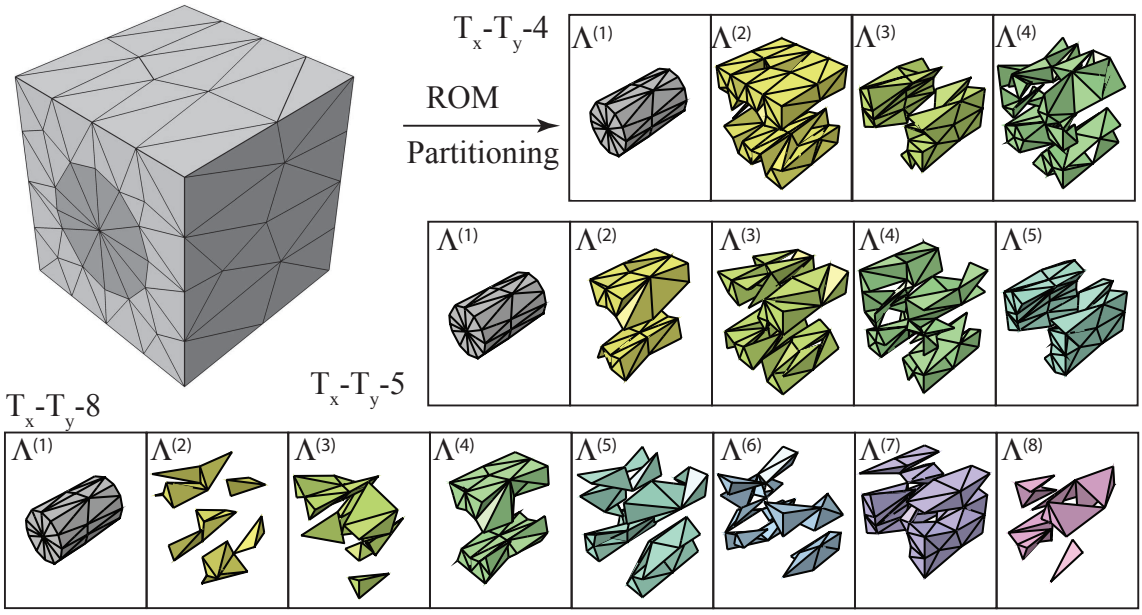

Figure 7: Optimal reduced order model partitionings for models T$_x$-T$_y$-4, T$_x$-T$_y$-5 and T$_x$-T$_y$-8.

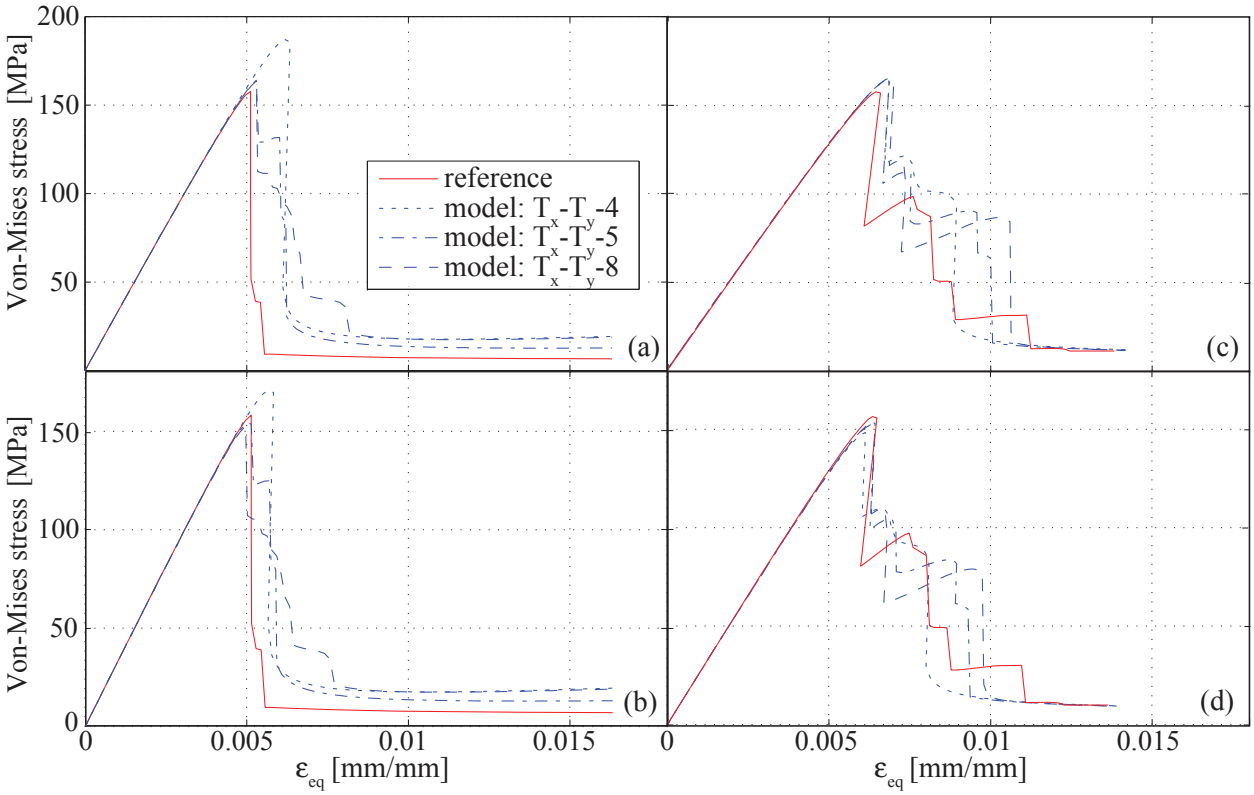

Figure 8: Von-Mises stress- equivalent strain curves: (a) unscaled models subjected to unaxial tension in y-direction, (b) parameter scaled models subjected to unaxial tension in y-direction, (c) unscaled models subjected to biaxial loading, and (d) parameter scaled models subjected to biaxial loading.

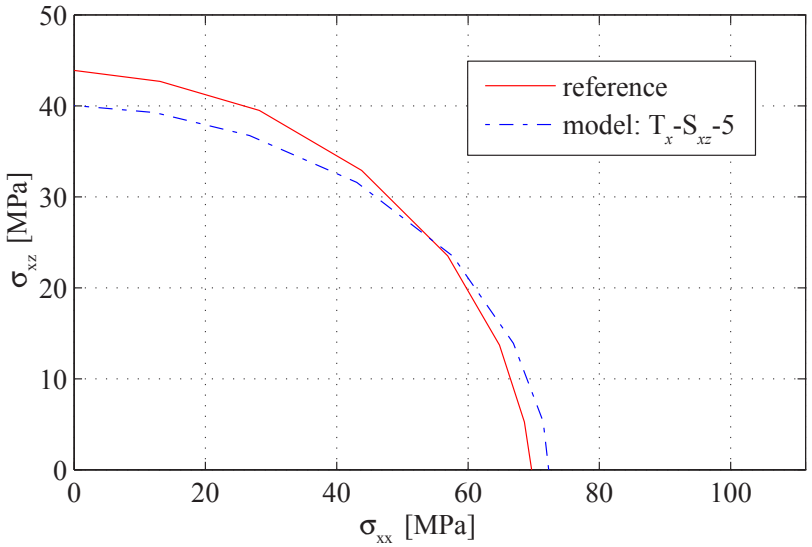

Figure 9: Failure envelope for model T_x-S_{xz}-5 when subjected to transverse tensile and shear loading.

$b^{(f)} = 300$ for the fiber phase.

We consider the reduced order model T_x-S_{xz}-5, which is identified under the uniaxial tensile loading in the transverse direction and shear ($n_{load} = 2$). A single part is assigned to the fiber phase since a sudden fiber failure that predominate the strength in the reinforcement direction is very well captured by a single part. Figure 9 shows the two-dimensional failure envelope along the combined transverse normal and shear directions as computed using T_x-S_{xz}-5 and the reference computational homogenization model. The parameter scaling constants for the fiber and matrix parts are 1.0 and 0.69, respectively. The reduced order model provides a good approximation to the reference model. Figure 10 shows the three-dimensional failure envelope as computed by the reference (Fig. 10a) and the reduced order (Fig. 10b) models for combined biaxial tensile and shear loading configurations. The predictions of T_x-S_{xz}-5 for all possible loading scenarios are satisfactory when compared to the reference solution. The predictions of the stress-strain response of the reduced order model are compared to the computational homogenization model in Fig. 11. The stress-strain response when the material is subjected to loading in the reinforcement direction is naturally dominated by the fiber behavior (Fig. 11a). More complex matrix dominated failure is observed at loading in the transverse (Fig. 11b), shear (Fig. 11c) and biaxial loading along the reinforcement and transverse directions with applied displacement ratio of $g_x/g_z = 0.75$ (Fig. 11d).

6 Conclusions

This manuscript presented a strategy for identifying optimal reduced order models for inelastic and failure response in heterogeneous materials. The reduced order modeling approach in this study is the eigendeformation-based reduced order homogenization method. The identification of the optimal reduced order model is posed as an integer optimization problem and the genetic algorithm method is used to evaluate the optimization problem. A series of numerical simulations were conducted to assess the performance of the identified reduced order

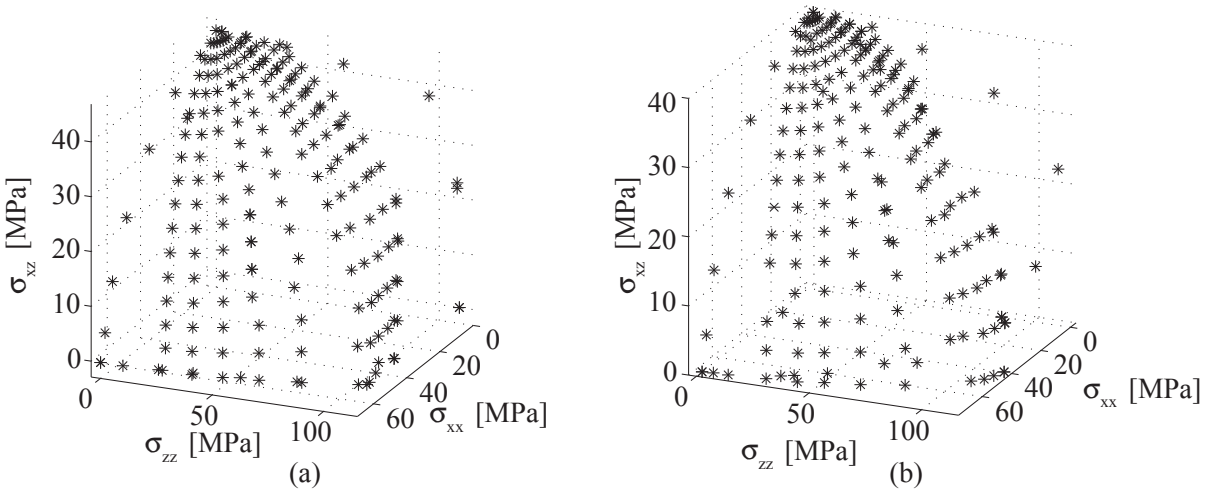

Figure 10: Three dimensional failure envelopes when subjected to combined tensile loading in reinforcement and transverse directions, and shear: (a) the reduced order model, T_x-S_{xz}-5; and, (b) the reference model.

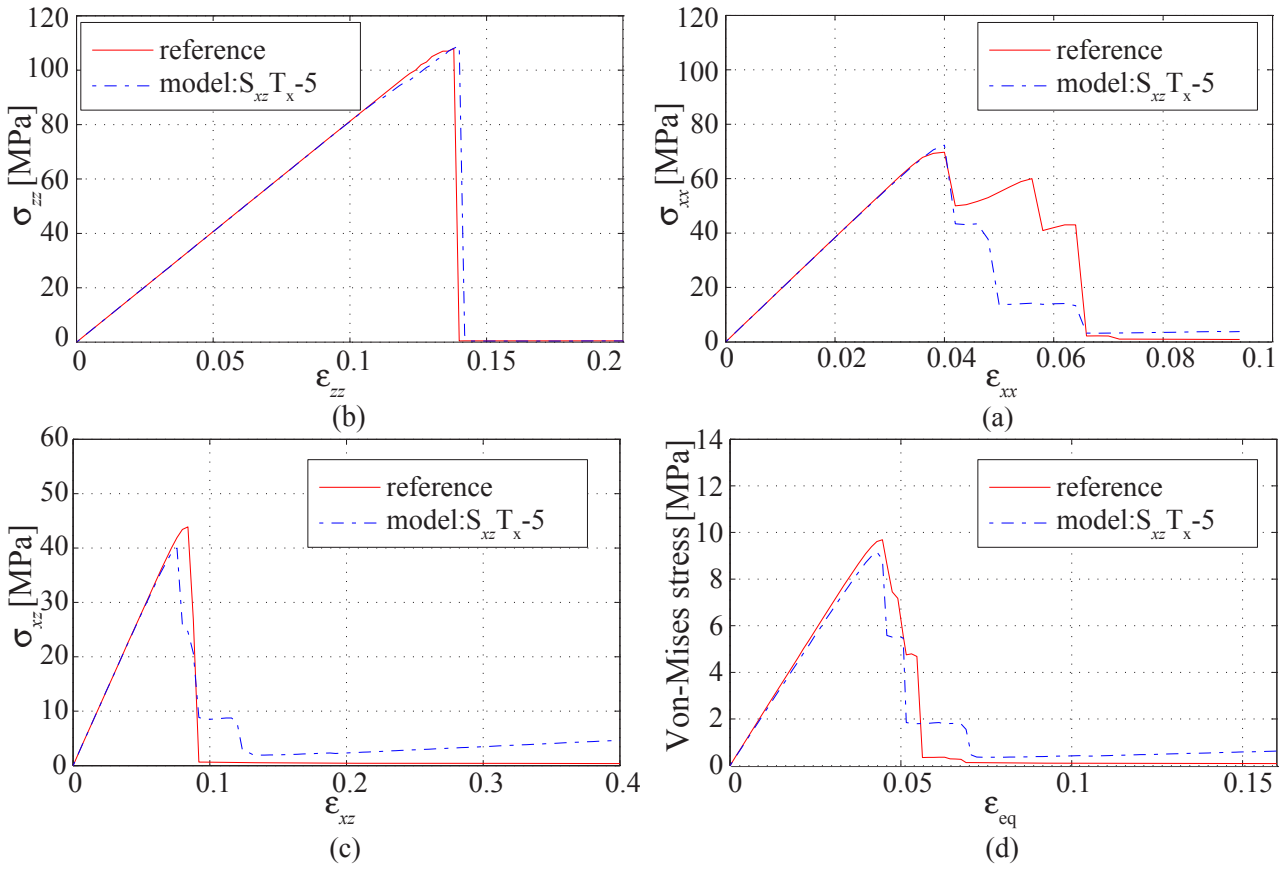

Figure 11: Stress-strain curves when subjected to: (a) uniaxial tension in the reinforcement direction; (b) uniaxial tension in the transverse direction; (c) shear, and (d) biaxial tension in the reinforcement and transverse directions.

models against the computational homogenization method, which considers full resolution of the material microstructure. Since the reduced order models are derived from the computational homogenization formulation in eigendeformation-based reduced order homogenization, the accuracy characteristics of the reduced order models are bounded by the computational homogenization method. The reduced order models identified using the proposed methodology are able to accurately capture the failure response characteristics for a wide range of loading conditions in our investigations. The failure response using relatively small order models were found to be satisfactory. The errors do not monotonically reduce by increasing the model order. This is attributed to possible identification of reduced order models at local minima of the objective function and the constraint imposed on high order models that preclude lower order models from being represented identically by the high order models in the model hierarchy. While the proposed methodology is effective in identifying satisfactory reduced order models, some issues remain to be addressed. The parameter scaling for the materials that exhibit more complex microconstituent response characteristics call for a different identification approach than employed in this study. Constitutive models for more complex material behavior include multiple material parameters, and the decision of which parameters needs to be scaled is model specific. The increase in computational complexity of the identification problem when the material microstructure is highly resolved remains outstanding. When the microstructure is densely meshed, the search space for the identification problem becomes very large and the interrogation of the search space with the posed integer optimization problem is computationally exhaustive. The reduction of the search space for the reduced order models is critical for highly resolved material microstructures. The outstanding issues mentioned above will be investigated in the future.

7 Acknowledgements

The authors gratefully acknowledge the financial support of the Southern Regional Education Board and Vanderbilt University.

References

[1] I. Babuska. Homogenization and application. mathematical and computational problems. In B. Hubbard, editor, *Numerical Solution of Partial Differential Equations - III, SYNSPADE*. Academic Press, 1975.

[2] A. Benssousan, J. L. Lions, and G. Papanicolaou. *Asymptotic Analysis for Periodic Structures*. North-Holland, Amsterdam, 1978.

[3] P. M. Suquet. Elements of homogenization for inelastic solid mechanics. In E. Sanchez-Palencia and A. Zaoui, editors, *Homogenization Techniques for Composite Media*. Springer-Verlag, 1987.

[4] E. Sanchez-Palencia. *Non-homogeneous media and vibration theory*, volume 127 of *Lecture Notes in Physics*. Springer-Verlag, Berlin, 1980.

[5] J. Fish, K. L. Shek, M. Pandheeradi, and M. S. Shephard. Computational plasticity for composite structures based on mathematical homogenization: Theory and practice. *Comput. Meth. Appl. Mech. Engng.*, 148:53–73, 1997.

[6] F. V. Souza, D. H. Allen, and Y. Kim. Multiscale model for predicting damage evolution in composites due to impact loading. *Compos. Sci. Technol.*, 68:2624–2634, 2008.

[7] J. Fish and K. L. Shek. Finite deformation plasticity of composite structures: Computational models and adaptive strategies. *Comput. Meth. Appl. Mech. Engng.*, 172:145–174, 1999.

[8] V. Kouznetsova, M. G. D. Geers, and W. A. M. Brekelmans. Multi-scale constitutive modelling of heterogeneous materials with a gradient-enhanced computational homogenization scheme. *Int. J. Numer. Meth. Engng.*, 54:1235–1260, 2002.

[9] I. Ozdemir, W. A. M. Brekelmans, and M. G. D. Geers. Fe^2 computational homogenization for thermo-mechanical analysis of heterogeneous solids. *Comp. Meth. Appl. Mech. Engng.*, 198:602–613, 2008.

[10] K. Terada and Kurumatani M. Two-scale diffusion-deformation coupling model for material deterioration involving micro-crack propagation. *Int. J. Numer. Meth. Engng.*, 83:426–451, 2010.

[11] T. Massart, R. H. J. Peerlings, and M. G. D. Geers. Structural damage analysis of masonry walls using computational homogenization. *Int. J. Damage Mechanics*, 16:199–226, 2007.

[12] T. B. Belytschko, S. Loehnert, and J. H. Song. Multiscale aggregating discontinuities: a method for circumventing loss of material stability. *Int. J. Numer. Meth. Engng.*, 73:869–894, 2008.

[13] V. P. Nguyen, O. Lloberas-Valls, M. Stroeven, and L. J. Sluys. Computational homogenization for multiscale crack modeling implementational and computational aspects. *Int. J. Numer. Meth. Engng.*, 2011.

[14] F. Feyel and J.-L. Chaboche. Fe^2 multiscale approach for modelling the elastoviscoplastic behavior of long fiber sic/ti composite materials. *Comput. Methods Appl. Mech. Engrg.*, 183:309–330, 2000.

[15] Rahul and S. De. An efficient coarse-grained parallel algorithm for global-local multiscale computations on massively parallel systems. *Int. J. Numer. Meth. Engng.*, 82:379–402, 2010.

[16] C. Oskay. Two-level multiscale enrichment methodology for modeling of heterogeneous plates. *Int. J. Numer. Meth. Engng.*, 80:1143–1170, 2009.

[17] C. Oskay and G. Pal. A multiscale failure model for analysis of thin heterogeneous plates. *Int. J. Damage Mechanics*, 19:575–611, 2010.

[18] E. W. C. Coenen, V. G. Kouznetsova, and M. G. D. Geers. Computational homogenization for heterogeneous thin sheets. *Int. J. Numer. Meth. Engng.*, 83:1180–1205, 2010.

[19] B. Mercatoris and T. Massart. A coupled two-scale computational scheme for the failure of periodic quasi- brittle thin planar shells and its application to masonry. *Int. J. Numer. Meth. Engng.*, 85:1177–1206, 2011.

[20] S. Nemat-Nasser and M. Hori. *Micromechanics: Overall Properties of Heterogeneous Materials*. North-Holland, 1999.

[21] M. Gosz, B. Moran, and J. D. Achenbach. Matrix cracking in transversely loaded fiber composites with compliant interphases. In AMD-150/AD-32, editor, *Damage Mechanics in Composites*. ASME, 1992.

[22] S. Ghosh and S. Moorthy. Elastic-plastic analysis of arbitrary heterogeneous materials with the voronoi cell finite element method. *Comput. Methods Appl. Mech. Engng.*, 121:373–409, 1995.

[23] J. Aboudi. The generalized method of cells and high-fidelity generalized method of cells micromechanical models-a review. *Mech. Adv. Materials and Structures*, 11:329–366, 2005.

[24] H. Moulinec and P. Suquet. A numerical method for computing the overall response of nonlinear composites with complex microstructure. *Comput. Meth. Appl. Mech. Engng*, 157:69–94, 1998.

[25] L. V. Berlyand and A. G. Kolpakov. Network approximation in the limit of small interparticle distance of the effective properties of a high-contrast random dispersed composite. *Archive for Rational Mechanics and Analysis*, 159:179–227, 2001.

[26] J. Yvonnet and Q.-C. He. The reduced model multiscale method (R3M) for the non-linear homogenization of hyperelastic media at finite strains. *J. Comput. Phys.*, 223:341–368, 2007.

[27] H. Lamari, A. Ammar, P. Cartraud, G. Legrain, F. Chinesta, and F. Jacquemin. Routes for efficient computational homogenization of nonlinear materials using the proper generalized decompositions. *Arch. of Comput. Methods in Eng.*, 17:373–391, 2010.

[28] J. Fish, Q. Yu, and K. L. Shek. Computational damage mechanics for composite materials based on mathematical homogenization. *Int. J. Numer. Meth. Engng.*, 45:1657–1679, 1999.

[29] J. L. Chaboche, S. Kruch, J. F. Maire, and T. Pottier. Towards a micromechanics based inelastic and damage modeling of composites. *Int. J. Plasticity*, 17:411–439, 2001.

[30] J. C. Michel and P. Suquet. Computational analysis of nonlinear composite structures using the nonuniform transformation field analysis. *Comput. Meth. Appl. Mech. Engng*, 193:5477–5502, 2004.

[31] C. Oskay and J. Fish. Eigendeformation-based reduced order homogenization for failure analysis of heterogeneous materials. *Comp. Meth. Appl. Mech. Engng.*, 196:1216–1243, 2007.

[32] R. Crouch and C. Oskay. Symmetric meso-mechanical model for failure analysis of heterogeneous materials. *Int. J. Mult. Comp. Eng.*, 8:447:461, 2010.

[33] G. J. Dvorak. On uniform fields in heterogeneous media. *Proc. R. Soc. Lond. A*, 431:89–110, 1990.

[34] G. J. Dvorak. Transformation field analysis of inelastic composite materials. *Proc. R. Soc. Lond. A*, 437:311–327, 1992.

[35] J. C. Simo and J. W. Ju. Strain- and stress-based continuum damage models - i. formulation. *Int. J. Solids Structures*, 23:821–840, 1987.

[36] J. Nocedal and S. Wright. *Numerical Optimization*. Springer Verlag, 2nd edition, 2006.

[37] J. H. Holland. *Adaptation in Natural and Artificial Systems*. University of Michigan Press, Ann Arbor, MI, USA, 1975.

[38] D. E. Goldberg. *Genetic Algorithms in Search, Optimization, and Machine Learning*. Addison Wesley Longman, Inc., 1989.

[39] R. L. Haupt and S. E. Haupt. *Practical Genetic Algorithms*. Wiley-Interscience, 2004.

[40] L. Davis. *Handbook of Genetic Algorithms*. Thomson Publishing Group / Van Nostrand Reinhold Company, New York, USA, 1991.

[41] R. Poli, W. B. Langdon, and N. F. McPhee. *A Field Guide to Genetic Programming*. Creative Commons Attribution-Noncommercial- No Derivative Works 2.0, United Kingdom, 2008.